9-27-2008

High-Resolution Surveys Along the Hot Spot–Affected Galapagos Spreading Center: 1. Distribution of Hydrothermal Activity

Edward T. Baker

Rachel M. Haymon
University of California - Santa Barbara

Joseph A. Resing

Scott M. White
University of South Carolina - Columbia, swhite@geol.sc.edu

Sharon L. Walker

See next page for additional authors

Publication Info

Published in *Geochemistry, Geophysics, Geosystems*, Volume 9, Issue 9, 2008, pages 1-16.
Baker, E. T., Haymon, R. M., Resing, J. A., White, S. M., Walker, S. L., Macdonald, K. C., Nakamura, K. (2008). High-resolution surveys along the hot spot–affected Galapagos Spreading Center: 1. Distribution of hydrothermal activity. *Geochemistry, Geophysics, Geosystems, 9* (9), 1-16.

Author(s)
Edward T. Baker, Rachel M. Haymon, Joseph A. Resing, Scott M. White, Sharon L. Walker, Ken C. Macdonald, and Ko-ichi Nakamura

Geochemistry Geophysics Geosystems G3
AN ELECTRONIC JOURNAL OF THE EARTH SCIENCES
Published by AGU and the Geochemical Society

Article
Volume 9, Number 9
27 September 2008
Q09003, doi:10.1029/2008GC002028
ISSN: 1525-2027

High-resolution surveys along the hot spot–affected Galápagos Spreading Center: 1. Distribution of hydrothermal activity

Edward T. Baker
Pacific Marine Environmental Laboratory, NOAA, 7600 Sand Point Way NE, Seattle, Washington 98115, USA (edward.baker@noaa.gov)

Rachel M. Haymon
Department of Geological Sciences and Marine Science Institute, University of California, Santa Barbara, Santa Barbara, California 93106, USA

Joseph A. Resing
Joint Institute for the Study of Atmosphere and Ocean, University of Washington, Seattle, Washington, USA

Pacific Marine Environmental Laboratory, NOAA, 7600 Sand Point Way NE, Seattle, Washington 98115, USA

Scott M. White
Department of Geological Sciences, University of South Carolina, Columbia, South Carolina 29205, USA

Sharon L. Walker
Pacific Marine Environmental Laboratory, NOAA, 7600 Sand Point Way NE, Seattle, Washington 98115, USA

Ken C. Macdonald
Department of Geological Sciences and Marine Science Institute, University of California, Santa Barbara, Santa Barbara, California 93106, USA

Ko-ichi Nakamura
National Institute of Advanced Industrial Science and Technology, Tsukuba Central 7, Higashi 1-1-1, Tsukuba, Ibaraki, 305-8567, Japan

[1] The spatial density of hydrothermal activity along most mid-ocean ridges is a robust linear function of spreading rate (or magmatic budget), but extreme crustal properties may alter this relationship. In 2005–2006 we tested the effect of thickened crust on hydrothermal activity using high-resolution mapping of plumes overlying the hot spot–affected Galápagos Spreading Center from 95° to 89°42′W (~560 km of ridge crest). Plume mapping discovered only two active, high-temperature vent fields, subsequently confirmed by camera tows, though strong plume evidence indicated minor venting from at least six other locations. Total plume incidence (p_h), the fraction of ridge crest overlain by significant plumes, was 0.11 ± 0.014, about half that expected for a non–hot spot mid-ocean ridge with a similar magmatic budget. Plume distributions on the Galápagos Spreading Center were uncorrelated with abrupt variations in the depth of the along-axis melt lens, so these variations are apparently not controlled by hydrothermal cooling differences. We also found no statistical difference (for a significance level of 0.05) in plume incidence between where the seismically imaged melt lens is shallow (2 ± 0.56 km, p_h = 0.108 ± 0.045) and where it is deep (3.4 ± 0.7 km, p_h = 0.121 ± 0.015). The Galápagos Spreading Center thus joins mid-ocean ridges near the Iceland (Reykjanes Ridge), St. Paul-Amsterdam (South East Indian Ridge), and Ascension (Mid-

Atlantic Ridge) hot spots as locations of anomalously scarce high-temperature venting. This scarcity implies that convective cooling along hot spot–affected ridge sections occurs primarily by undetected diffuse flow or is permanently or episodically reduced compared to normal mid-ocean ridges.

Components: 8729 words, 8 figures, 1 table.

Keywords: hydrothermal venting; mantle hot spot; Galápagos spreading ridge.

Index Terms: 8424 Volcanology: Hydrothermal systems (0450, 1034, 3017, 3616, 4832, 8135); 8416 Volcanology: Mid-oceanic ridge processes (1032, 3614); 3037 Marine Geology and Geophysics: Oceanic hotspots and intraplate volcanism.

Received 11 March 2008; **Revised** 2 June 2008; **Accepted** 9 June 2008; **Published** 27 September 2008.

Baker, E. T., R. M. Haymon, J. A. Resing, S. M. White, S. L. Walker, K. C. Macdonald, and K. Nakamura (2008), High-resolution surveys along the hot spot–affected Galápagos Spreading Center: 1. Distribution of hydrothermal activity, *Geochem. Geophys. Geosyst.*, *9*, Q09003, doi:10.1029/2008GC002028.

1. Introduction

[2] This investigation is another in a continuing effort to explore the relationship between hydrothermal venting and extreme crustal properties [e.g., *Baker et al.*, 2004]. Ridge sections that neighbor or intersect "hot spots," localized centers of excess magmatic, geochemical, or thermal anomalies, are distinguished by crust significantly thicker than the mid-ocean ridge (MOR) standard of ~6–7 km [*White et al.*, 1992; *Chen*, 1992]. Hot spots were identified early in the plate tectonic revolution and initially ascribed to buoyantly rising melt from deep within the mantle [*Wilson*, 1963; *Morgan*, 1971]. While some hot spots may arise from deep mantle plumes, alternative explanations include shallow melting anomalies, such as excess melting under hydrous conditions in the upper mantle [*Schilling et al.*, 1980; *Cushman et al.*, 2004], and simple seepage of mantle melt through lithospheric cracks [e.g., *Anderson et al.*, 1992; *Courtillot et al.*, 2003]. Regardless of origin, about 40 "hot spot–like" features dot the ocean, half of which are close enough to MORs to influence their bathymetry and/or geochemistry [*Ito et al.*, 2003; *Courtillot et al.*, 2003; *Dyment et al.*, 2007].

[3] Analysis of along-axis bathymetric and gravity anomalies has found that hot spots can exert a measurable influence on MORs from a distance of at least 500 km [*Ito and Lin*, 1995]. Bathymetric anomalies along MORs are created by thickened crust and lower density lithosphere beneath the seafloor. Modeling often suggests that this material is hotter than normal mantle by several 10s of degrees [e.g., *Ito and Lin*, 1995], though a temperature anomaly is not required at all ridge sites where a bathymetric anomaly is observed [e.g., *Bruguier et al.*, 2003].

[4] If a hot spot influence significantly alters the crustal properties of a ridge, hydrothermal circulation within the crust may be affected as well. Exploration for hydrothermal activity along ridge sections affected by the Iceland (Reykjanes Ridge), St. Paul-Amsterdam (South East Indian Ridge (SEIR)), and Ascension (southern Mid-Atlantic Ridge (MAR)) hot spots have found fewer hydrothermal plumes compared to other MORs of similar spreading rate [*Baker and German*, 2004; *Devey et al.*, 2005]. These observations suggest that hydrothermal cooling along hot spot–affected ridge sections is reduced, or expressed differently, than along other MORs. The hot spot–affected GSC provides an ideal natural laboratory to test this hypothesis, since over a span of ~450 km from 91° to 95°W it grades from thicker crust underlain by a warmer mantle to crust of normal thickness and temperature [*Canales et al.*, 2002]. Accordingly, we conducted the most rigorous exploration for hydrothermal activity yet completed on any hot spot–affected ridge section. A continuous, dual-pass water column survey for hydrothermal plumes covered 564 km of the GSC, spanning that portion of the ridge where the hot spot influence is most pronounced (Figure 1) [*Canales et al.*, 2002; *Detrick et al.*, 2002; *Christie et al.*, 2005]. Here, we report the distribution of hydrothermal plumes and then compare the results to those from other, less comprehensive, surveys over other hot spot–influenced ridge sections. Finally, we evaluate several reasons why detectable hydrothermal

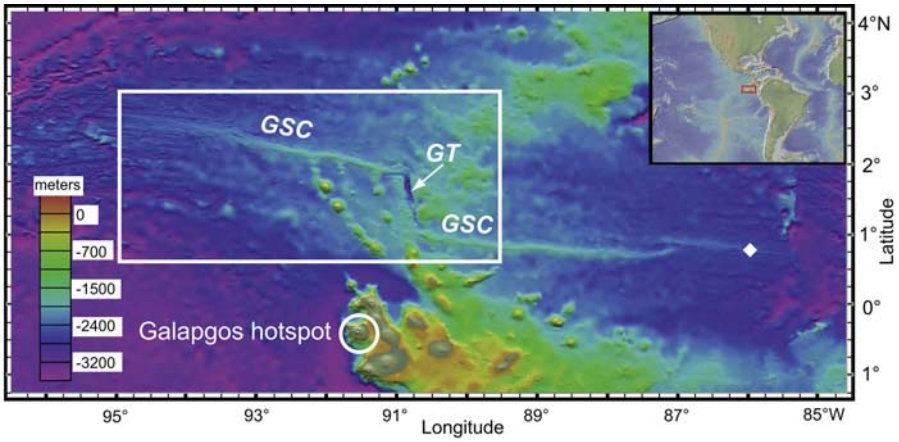

Figure 1. Location map of the Galápagos region. White box outlines the study area, encompassing the Galápagos Spreading Center (GSC) and the Galápagos Transform (GT). Solid diamond identifies the Rose Garden vent field, discovered in 1977 [*Corliss et al.*, 1979]. The Galápagos hot spot is thought to presently underlie Fernandina Island.

plumes along these ridge sections might be reduced compared to normal MORs.

2. Methods

[5] Water column investigations were conducted in conjunction with fine-scale bathymetric mapping using a deep-towed side-scan sonar vehicle. Hydrothermal plumes were mapped by a combination of autonomous sensors on the tow wire of the DSL-120A sonar system, real-time sensors on the DSL-120A clump weight, and targeted conductivity-temperature-depth-optical (CTDO) tow-yos. Along the western GSC, two roughly parallel DSL-120A lines were run between 91°05′ and 94°57′W to fully image the ridge axis, while a single line was run from 90°38′ to 89°35′W along the eastern limb (Figure 2 and Table 1) [*White et al.*, 2008; *Haymon et al.*, 2008]. Twenty CTDO tows covered ~140 km of axis length and were supplemented by 13 vertical casts, including three at volcanic constructs within the Galápagos Transform. A suite of eight Miniature Autonomous Plume Recorders (MAPRs) [*Baker and Milburn*, 1997] with optical backscattering sensors were attached above and below the DSL-120A clump weight, spanning the water column from ~60 to ~300 m above bottom for a nominal clump weight altitude of 110 m. MAPRs recorded pressure, temperature, and light backscattering every 10 s, about every 10 m along track, for ~1000 km of track line, with 46 of 49 deployments fully successful. Light backscattering is reported as nephelometric turbidity units (NTU) [*American Public Health Association*, 1985]; ΔNTU is the value above ambient, nonplume water.

[6] The clump weight itself was instrumented with an in situ chemical analyzer for Fe and Mn [*Massoth et al.*, 1998], an additional optical backscatter sensor, and an oxidation-reduction potential (ORP), sometimes called Eh, detector. The ORP instrument measures the equilibrium electrode potential, E, ranging from −0.5 to +0.5 V, between a Pt electrode in seawater and an Ag-AgCl reference electrode in a saturated KCl solution. An E value of about 0.25 V is typical for ambient seawater. Lower voltages relative to ambient water (ΔE) are indicative of reduced hydrothermal species, including H_2S and Fe^{+2} [*Walker et al.*, 2007; J. A. Resing, unpublished data, 2007], and thus its response is roughly inversely proportional to plume "age" as these species are oxidized and diluted while mixing with ambient seawater. E profiles (horizontal or vertical) are markedly asymmetric, characterized by an often-instantaneous reduction in E upon entering a plume, followed by a slow recovery to ambient values after leaving a plume. Absolute values of E are thus not always comparable from site to site because equilibrium of the detector to local conditions may take many minutes and may not completely return to the original background value; in that sense the instrument is more properly a detector than a sensor.

[7] Hydrothermal plumes were identified from MAPR ΔNTU anomalies, ΔE anomalies from the single detector on the clump weight (altitude ~110 m), and from ΔNTU, ΔE, and hydrothermal temperature anomalies from the CTDO tows. In all cases but that of a single spatially restricted plume, follow-up CTDO tows confirmed the MAPR-detected plumes. Some minor plumes were identified only by MAPR ΔNTU, presumably because

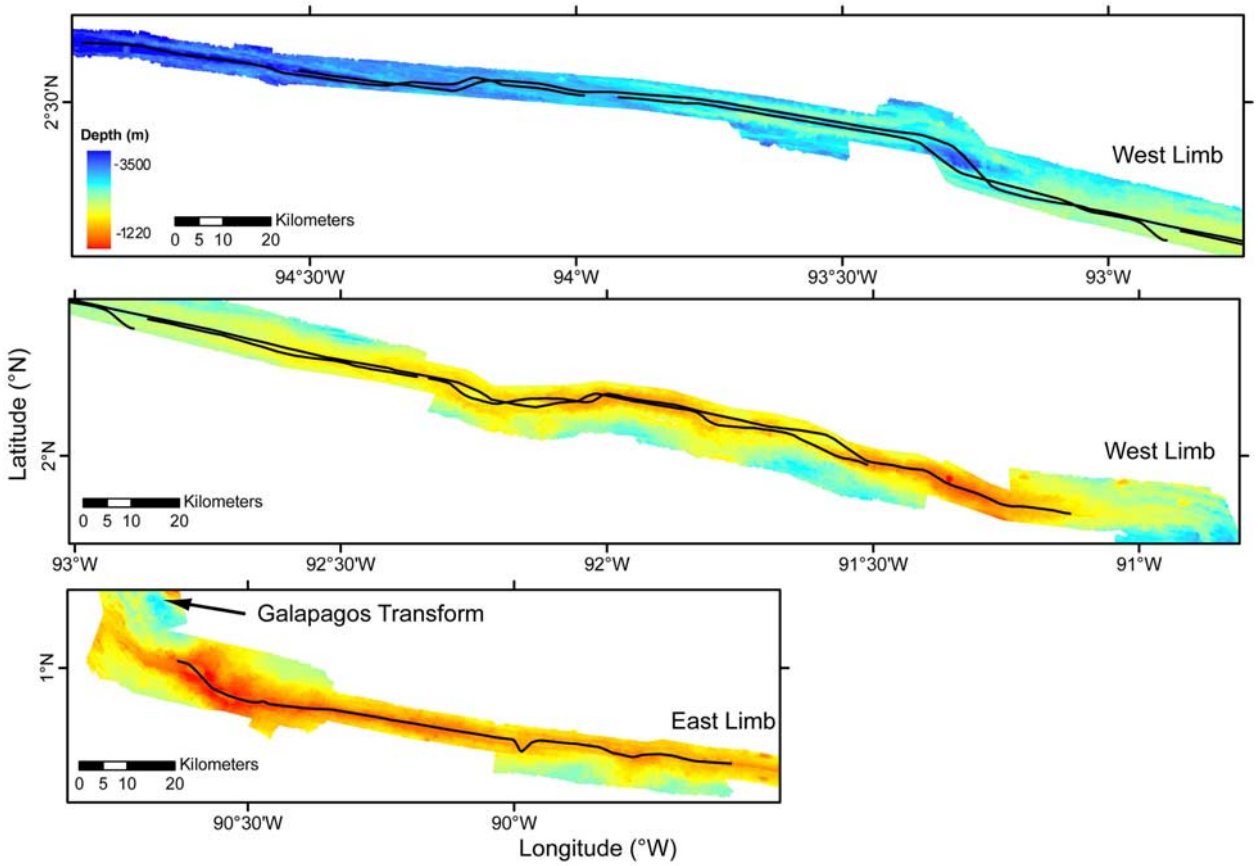

Figure 2. GSC axial bathymetry overlain by the DSL-120A/MAPR tow tracks (black lines).

some plumes were above or below the clump weight altitude. Other plumes were apparent only from the clump weight ΔE detector, evidently because some low-temperature discharge might have had a weak or negligible optical signal. Some detector responses are most likely not hydrothermal, such as ΔNTU from resuspension or ΔE spikes from suspended organic particles that impact the ORP detector.

3. Geologic Setting

[8] The Galápagos hot spot lies 100–200 km south of the GSC (Figure 1), close enough to

Table 1. DSL-120A/MAPR Deployment Log

Segment	DSL Deployment	Lat. (°N)	Long. (°W)	Date[a]	Time (UTC)	Distance (km)
West Limb, west to east	DSL-1 (start)	2°34.1′	94°35′	06/12/2005	00:58	
	DSL-1 (end)	2°31.7′	94°17.9′	06/12/2005	16:30	31
	DSL-2 (start)	2°32.1′	94°21′	07/12/2005	04:01	
	DSL-2 (end)	1°53.2′	91°08.1′	13/12/2005	07:00	351
East Limb, west to east	DSL-3 (start)	1°00.8′	90°38.2′	16/12/2005	20:46	
	DSL-3 (end)	0°49.8′	89°34.6′	18/12/2005	14:30	116
West Limb, east to west	DSL-4 (start)	1°52.7′	91°03.2′	20/12/2005	11:31	
	DSL-4 (end)	1°54.3′	91°14.2′	20/12/2005	18:50	20
	DSL-5 (start)	1°58.8′	91°30.2′	21/12/2005	16:01	
	DSL-5 (end)	2°15.8′	92°52.8′	23/12/2005	19:35	150
	DSL-6 (start)	2°14.6′	92°52.9′	24/12/2005	04:01	
	DSL-6 (end)	2°36.7′	94°56.4′	27/12/2005	19:19	225

[a] Read 06/12/2005 as 6 December 2005.

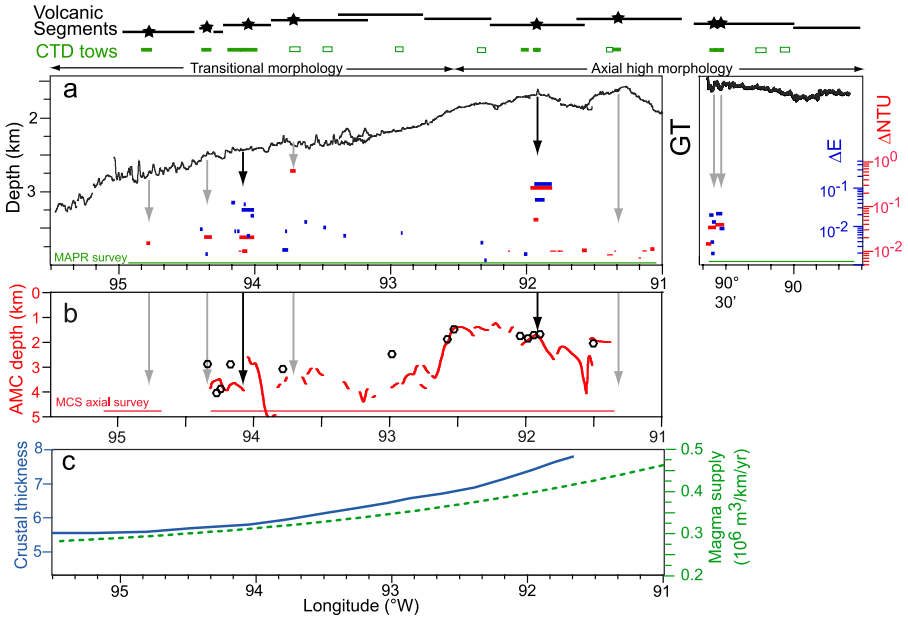

Figure 3. (a) Bathymetric cross-section of the GSC in our study area. The Galápagos hot spot influence is centered near the Galápagos Transform (GT), where it creates a shallow ridge and axial high morphology. Location and intensity of ΔNTU (red lines) and ΔE (blue lines) plume anomalies are plotted beneath the bathymetry; logarithmic scales for each are at far right. Thin lines indicate that the ΔNTU anomaly was seen only on the lowermost MAPR (∼50 mab); all other ΔNTU anomalies were detected on multiple MAPRs. Black vertical arrows show vent sites confirmed by camera tows (Haymon et al., submitted manuscript, 2008); gray arrows show sites where plume data strongly suggest active venting. At the panel top are shown the location of CTD tows, solid where plumes were detected and hollow where not detected, and the volcanic segmentation (White et al., submitted manuscript, 2008), with stars marking confirmed and possible vent sites. (b) Red profile traces the depth of the AMC from along-axis seismic lines, and hexagons mark the depth from cross-axis seismic lines [*Detrick et al.*, 2002; *Blacic et al.*, 2004]. (c) Magma supply (green dotted line) and crustal thickness (blue solid line) both increase toward the maximum hot spot influence [*Canales et al.*, 2002; *Sinton et al.*, 2003].

strongly impact the ridge without overwhelming its MOR characteristics. Maximum influence is centered on the ridge sections adjacent to the Galápagos Transform at 91°W [*Canales et al.*, 2002; *Detrick et al.*, 2002; *Sinton et al.*, 2003; *Christie et al.*, 2005; R.M. Haymon et al., submitted manuscript, 2008; White et al., submitted manuscript, 2008]. Axial high morphology stretches from 89°10′ to 92°30′W, with an axial depth of <1900 m (Figure 3a). Westward of the axial high region lies a transitional morphology, neither axial high nor axial valley, deepening to ∼2750 m at 95°W. An axial magma chamber (AMC) is commonly present between 91°20′ and 94°20′W, but unseen farther west [*Detrick et al.*, 2002; *Blacic et al.*, 2004] (no seismic studies are available from the eastern limb) (Figure 3b). The AMC is shallow (2 ± 0.56 km) and nearly continuous beneath the axial high morphology on the western limb, but deepens sharply to the west (3.4 ± 0.7 km) and becomes more discontinuous as the axial morphology becomes transitional.

[9] Mirroring the axial depth, on-axis crustal thickness decreases from >8 km at 91°40′W to <6 km at 95°W [*Canales et al.*, 2002] as the magma supply rate declines by a third [*Sinton et al.*, 2003] (Figure 3c). *Canales et al.* [2002] calculate that the Galápagos bathymetric anomaly arises about equally from crustal thickening and reduced mantle density, implying a mantle temperature anomaly (ΔT) of ∼30°C. A petrological model suggests ΔT may be as low as ∼20°C [*Cushman et al.*, 2004]. Spreading rates vary little across the study area, increasing from 52 mm/a at 95°W to 60 mm/a at 89°W [*DeMets et al.*, 1994].

4. Plume Distributions

[10] The GSC is remarkably devoid of hydrothermal plumes compared with other intermediate- and fast-rate ridge sections of similar length. This condition is easily visualized by plotting ΔNTU versus longitude for all MAPRs along a single transect of the western limb (Figure 4). ΔNTU

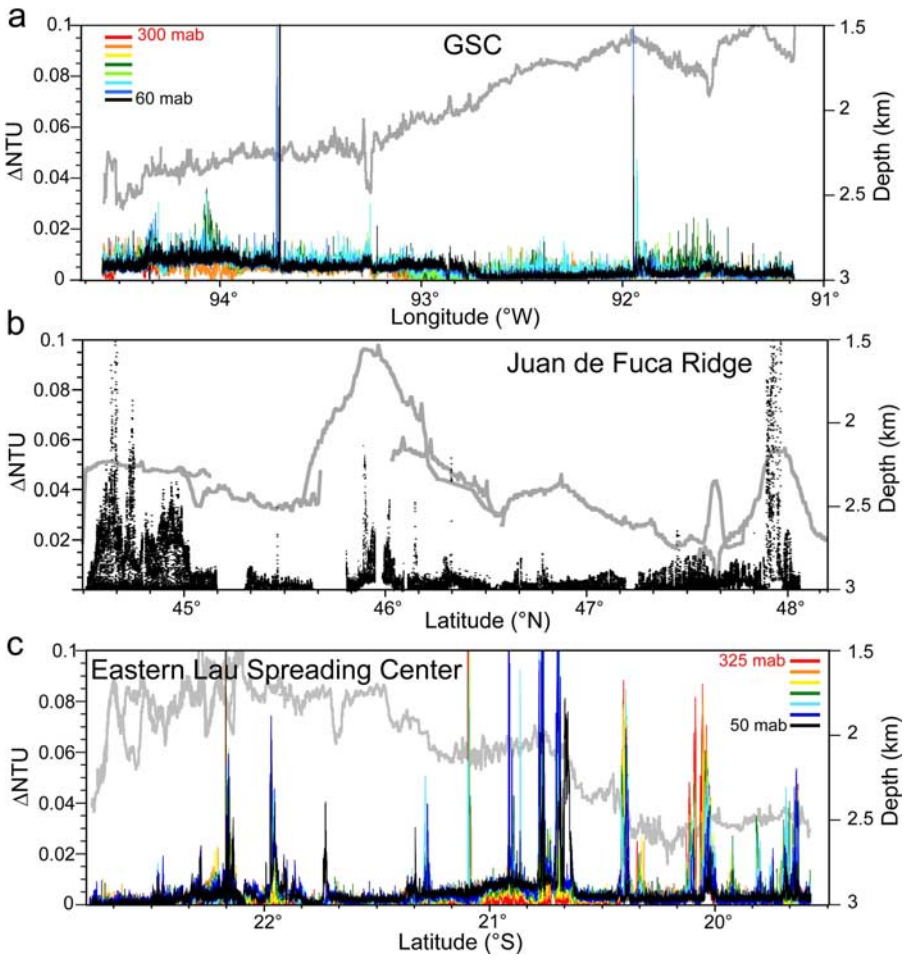

Figure 4. Comparison of the frequency and intensity of optical (ΔNTU) plumes along (a) the GSC, (b) the Juan de Fuca Ridge [*Baker and Hammond*, 1992; E.T. Baker, unpublished data, 1998], and (c) the Eastern Lau Spreading Center [*Baker et al.*, 2006]. The GSC and Lau data sets were compiled from a similar array of MAPRs on the deep-towed DSL-120, positioned at comparable meters above bottom (mab). The JdFR data set is compiled from a series of CTDO tow-yos. The gray curve in each panel is axial depth. The *y* axis scales are identical in each panel.

values substantially exceed background (~0.005 to 0.01, depending on location) only near 91°55′, 93°42′, 94°05′, and 94°20′W. The prominent rise in baseline ΔNTU values west of 92°40′ corresponds to the abrupt deepening and widening of the axial graben (White et al., submitted manuscript, 2008), apparently creating enough relief to trap a weak bottom nepheloid layer. The GSC plume incidence is clearly less in both extent and magnitude than that found on the intermediate-rate (55 mm/a) Juan de Fuca Ridge, where plumes were mapped using the standard CTDO tow-yo method [*Baker and Hammond*, 1992]. The difference is even more striking along the back-arc Eastern Lau Spreading Center. Here spreading rates of 40–90 mm/a bracket that of the GSC and plumes were mapped using the same methodology as used on the GSC [*Baker et al.*, 2006].

4.1. Confirmed Vent Fields

[11] Active, high-temperature discharge was confirmed at two locations where camera tows imaged black smoker chimneys (Haymon et al., submitted manuscript, 2008). The largest field included the "Iguanas" and "Pinguinos" sites between 91°48′ and 91°56′W, and may stretch farther east on the basis of weaker but persistent plume signals (Figure 5a). On both transects the highest rising plumes and most intense ΔNTU and ΔE anomalies were found between 91°56.4′ and 91°54.6′W (Figure 5a). Five clusters of actively discharging vents and several sparsely populated faunal communities were imaged by the camera surveys in this area.

[12] The other confirmed field is "Navidad," where smokers and a thriving community of biota

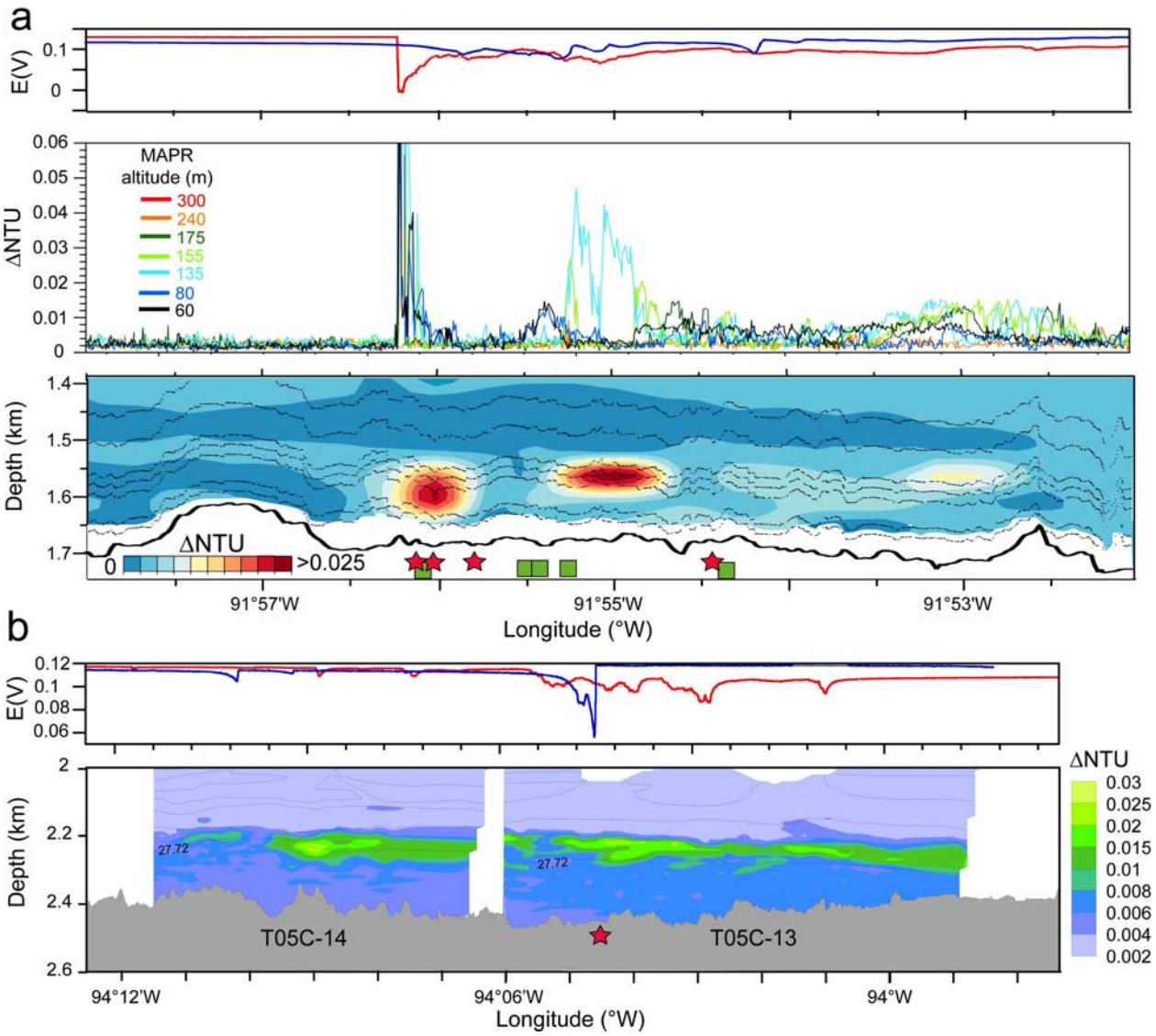

Figure 5. (a) Hydrothermal plumes over the Iguanas/Pinguinos vent field. Top panel shows profiles of E from DSL-2 (red line) and DSL-6 (blue line). As apparent during DSL-2, moving west to east, the ORP detector reacts quickly upon encountering reduced chemicals but has a slow recovery to background values. Middle panel shows individual MAPR records, color coded to depth above bottom. Bottom panel shows the same data contoured; parallel lines above the seafloor indicate the MAPR paths. Red stars are active vents, and green boxes are vent faunal communities imaged by a camera survey (91°53.5′–56.5′W) (Haymon et al., submitted manuscript, 2008). (b) Hydrothermal plumes over the Navidad vent field (94°04.5′W) (Haymon et al., submitted manuscript, 2008). Top panel shows profiles of E from DSL-2 (red line) and DSL-6 (blue line). Bottom panel shows contoured ΔNTU data from CTDO tow-yos showing a strong plume layer extending for >20 km at a depth of ∼2200–2300 m. Potential density isopycnals are overlain. Red star is the active vent. Note change in ΔNTU color scale compared to Figure 5a.

were imaged at 94°04.5′W (Haymon et al., submitted manuscript, 2008). Strong ΔNTU and ΔE anomalies produced a continuous plume stretching >20 km between 94°11′ and 94°W (Figure 5b).

4.2. Inferred Fields

[13] We also infer active discharge at several locations where we either imaged no vents or conducted no camera tows. On the eastern limb, strong indications of venting were recorded within both of the Los Huellos calderas that sit astride the axial high between 90°37′ and 90°30′W (Figure 6) [*Christie et al.*, 2005; White et al., submitted manuscript, 2008; Haymon et al., submitted manuscript, 2008]. We observed weak but consistent ΔNTU anomalies close to the northern and eastern

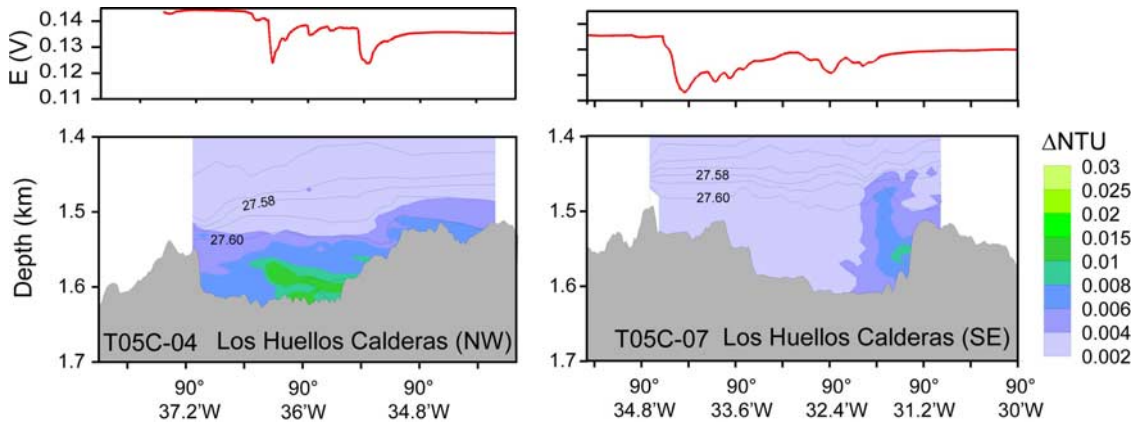

Figure 6. Hydrothermal plumes over the Los Huellos calderas on the east limb of the GSC. (top) Profiles of E from DSL-3. (bottom) Contoured ΔNTU data from CTDOs through the calderas. The CTDO towpaths closely followed the DSL towpath. Potential density isopycnals are overlain.

walls in both calderas. Discrete samples with substantially increased ^{3}He and Mn concentrations confirm a hydrothermal origin [*Resing et al.*, 2006]. The only discrete vents found during a 48-h camera survey in the eastern caldera were long-extinct chimneys on the caldera rim (Haymon et al., submitted manuscript, 2008). This camera tow also encountered cloudy water, suspended floc, ΔE anomalies, and hydrothermal sediments on the caldera floor, all strong evidence of active diffuse flow.

[14] On the western limb, we observed coincident optical and chemical plume anomalies at several sites (Figure 7). Along the axial high morphology at 91°17–24′W, MAPRs on DSL-1 found very weak and uncertain ΔNTU anomalies, but CTDO tow T05C-10 identified a small area of near-bottom ΔNTU and ΔE anomalies (Figure 7a). A near-bottom sample (at 91°18′W) found elevated total Mn (18 nM) and total S (39 nM) [*Resing et al.*, 2006]. Camera tows imaged a field of apparently inactive chimneys nearby at 91°24′W (Haymon et al., submitted manuscript, 2008).

[15] From 93°42′ to 43′W, DSL-2 recorded intense but spatially restricted ΔNTU anomalies. As the tow proceeded eastward, a ΔNTU peak was first seen at 93°43.2′W at an altitude of 110 m, then on only two MAPRs between ~80 and 135 m altitude about 1 km farther downtrack, and then at ~60 and 80 m altitude another 1.5 km distant (Figure 7b), finally reaching ΔNTU = 0.6, the highest recorded during the cruise. This pattern indicates a plume sourced near 2°30′N, 93°42′W and rising as it was advected westward. The plume was not detected on a second tow (DSL-6), nor on two CTDO tows deployed to sample it, so the field is likely small but almost certainly high temperature.

[16] At 94°20′–24′W, MAPRs on DSL-2 recorded a broad area of weak and low-lying ΔNTU anomalies, while the clump weight ORP detector (but not the optical sensor), observed a sequence of individual anomalies. CTDO tow T05C-01 through the same area mapped ΔNTU and ΔE anomalies between 94°21′ and 94°22′W (Figure 7c), plus total Mn concentrations as high as 12 nM coincident with the plume maxima [*Resing et al.*, 2006].

[17] Near 94°46′–47′W, DSL-6 recorded a series of weak ΔNTU inflections on several MAPRs. CTDO tow T05C-12 confirmed a plume between 94°48′ and 49′W (Figure 7d), including a ΔE anomaly and total Mn concentrations as high as 14 nM [*Resing et al.*, 2006].

4.3. Possible Fields

[18] This category includes sites where only one anomaly type, ΔNTU or ΔE, was observed and neither furnished compelling evidence of a hydrothermal plume. For example, at 91°04′W all MAPRs but the uppermost on DSL-4 showed slightly increased ΔNTU values immediately upon reaching the tow depth, but no ΔE anomaly accompanied this increase. At 93°46′W, ΔE anomalies were detected during both DSL-2 and DSL-6 (Figure 3). This location might host a low-temperature vent site discharging a particle-poor plume. Other locations, mostly small ΔE anomalies or ΔNTU anomalies seen on only a single MAPR, are shown in Figure 3.

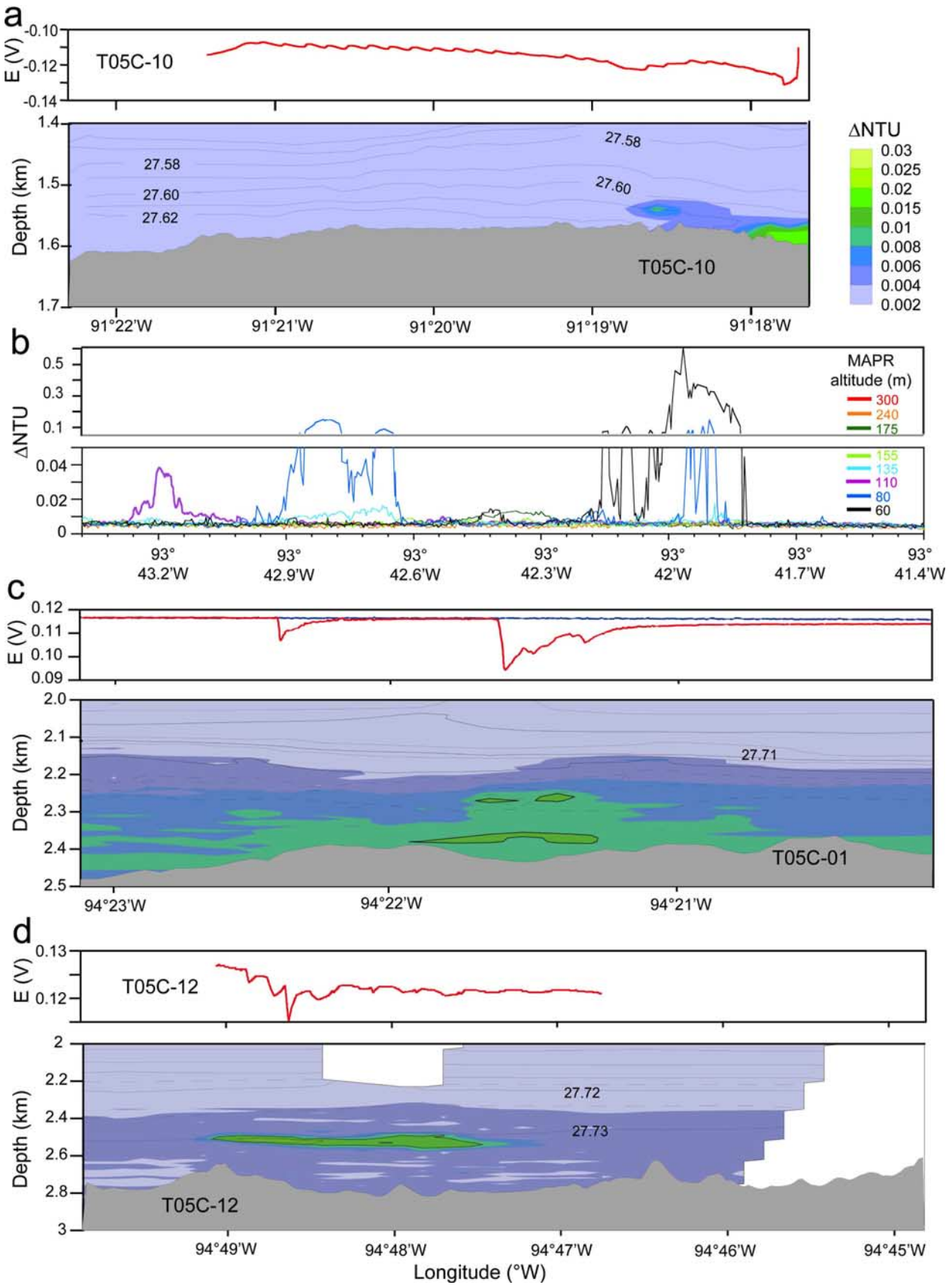
a
E (V)
T05C-10
Depth (km)
27.58
27.60
27.62
ΔNTU
0.03
0.025
0.02
0.015
0.01
0.008
0.006
0.004
0.002
91°22'W
91°21'W
91°20'W
91°19'W
91°18'W
b
ΔNTU
MAPR altitude (m)
300
240
175
155
135
110
80
60
93° 43.2'W
93° 42.9'W
93° 42.6'W
93° 42.3'W
93° 42'W
93° 41.7'W
93° 41.4'W
c
E (V)
Depth (km)
27.71
T05C-01
94°23'W
94°22'W
94°21'W
d
E (V)
T05C-12
Depth (km)
27.72
27.73
T05C-12
94°49'W
94°48'W
94°47'W
94°46'W
94°45'W
Longitude (°W)

Figure 7

4.4. Plume Distribution Summary

[19] Figure 3a summarizes the along-axis distribution of all plume anomalies detected by the DSL and CTDO tows. Eight locations show reliable evidence of hydrothermal activity, as described above. We use plumes only at these locations to calculate plume incidence, p_h, the fraction of ridge axis overlain by significant hydrothermal plumes [*Baker and Hammond*, 1992]. (Including the questionable plume evidence at other locations would insignificantly increase p_h since their total along-axis extent is small.) For the entire study area p_h = 0.109 with an uncertainty of ±0.014. This uncertainty is based on the dual-pass mapping of the west limb. DSL-1 and -2 and CTDO tow-yos yielded a p_h = 0.134, while DSL-4 to -6 and CTDO tow-yos yielded a p_h = 0.098. The east limb p_h of 0.081 is based on DSL-3, and the east limb CTDO tow-yos. In all cases where DSL and CTDO tows covered the same area, the tows mapping the most extensive plume coverage were used in the p_h calculations.

[20] On a finer scale, p_h = 0.108 ± 0.045 along the region of the shallow AMC (91°–92°30′W), which is lower than the p_h of 0.121 ± 0.015 found over the deep AMC (92°30′–95°). This difference is not statistically significant (for a significance level of 0.05) given the uncertainty levels. If we assume that the eastern limb is underlain by an AMC with a depth comparable to that of the axial high portion of the western GSC and combine the two sections, the overall p_h for an axis section with a shallow AMC would decrease only negligibly to 0.102. Even if the difference between shallow and deep AMC regions was statistically significant, the low p_h values and the short lengths of ridge encompassed by the shallow and deep AMC would make any geological interpretation of the differences unreliable.

[21] It is interesting to compare the uniformity of the p_h values, as well as the scarcity of high ΔNTU plumes indicative of vigorous vent fields, with the surficial geological characteristics. Pillow flow lava morphology dominates the neovolcanic zone, and fissure density has no along-axis trend (about 2 km/km^2 throughout the west limb) except for a ∼10% increase where the AMC is deep (White et al., submitted manuscript, 2008). Pillow flows cover 90–100% of the side scan-imaged area between 95° and 91°30′W, a preponderance more similar to slow-rate ridges than to intermediate-rate ones [*Perfit and Chadwick*, 1998]. Only immediately adjacent to the Galápagos Transform (91°30′–91°W and 90°45′–90°30′W) do sheet flows reach even ∼20% coverage. All active vent sites imaged by camera tows are hosted in pillow lavas (Haymon et al., submitted manuscript, 2008).

[22] The only other location where a combined side scan and hydrothermal survey has attempted to correlate surficial fractures (fissures and faults) with venting is along the superfast spreading southern East Pacific Rise [*Hey et al.*, 2004]. Fissure/fault density there was inversely correlated with hydrothermal plumes, varying from high densities of ∼1 km/km^2 where plumes were mostly absent to <∼0.5 km/km^2 where plumes were most abundant. Areas of active venting often occurred where the areal density of lava sheet flows was greatest.

5. Comparisons to Other Hot Spot–Ridge Intersections

[23] Besides the GSC, five other MOR sections in the vicinity of hot spots or melting anomalies have been at least cursorily surveyed for hydrothermal activity: the Reykjanes Ridge (Iceland hot spot), the SEIR (St. Paul-Amsterdam), the southern MAR (Ascension), the Juan de Fuca Ridge (Cobb), and the northern MAR (Azores). Two of these, those near the Cobb and Azores hot spots, are unsuitable or not easily comparable to the remaining three for investigating changes in hydrothermal activity attributable to hot spot–ridge interactions. Cobb is unusual in that the bathymetric, crustal thickness, and mantle thermal anomalies are weak and limited to a 100-km-long segment of the Juan de Fuca

Figure 7. (a) (top) Profile of E from a CTDO tow between 91°17′ and 91°22′W. (bottom) Contoured ΔNTU data from the CTDO tow-yo shows near-bottom plumes near 91°18′W that correspond to ΔE anomalies. Potential density isopycnals are overlain. (b) Individual MAPR records near 93°42′W from DSL-2. Note the break in the *y* axis scale at 0.05 ΔNTU. MAPRs are color coded to depth above bottom. No ORP anomalies accompanied the ΔNTU anomalies. (c) (top) Profiles of E from DSL-1 (red line) and DSL-6 (blue line) between 94°21′ and 94°23′W. Anomalies were seen only during DSL-1. (bottom) Contoured ΔNTU data from a CTDO tow-yo shows a broad area of low-lying plumes corresponding to the ΔE anomalies detected during DSL-1. Potential density isopycnals are overlain. (d) (top) Profile of E from a CTDO tow between 94°47′ and 94°49′W. (bottom) Contoured ΔNTU data from the same CTDO tow-yo shows a plume corresponding to the ΔE anomalies. Potential density isopycnals are overlain.

Ridge centered on the ~700-m-high Axial Volcano [*Hooft and Detrick*, 1995; *West et al.*, 2003]. Hydrothermal activity on the segment is limited to the summit of Axial Volcano [*Baker and Hammond*, 1992; E. T. Baker, unpublished data, 1998] and appears to be controlled by a shallow melt reservoir [*West et al.*, 2001]. The volcano-dominated bathymetry and hydrothermal activity make this site unsuitable for examining the hydrothermal aspects of hot spot–ridge interaction.

[24] The Azores hot spot affects the basaltic chemistry of the northern MAR between ~40° and 33°30′N [e.g., *Schilling*, 1975], where five confirmed and at least five inferred hydrothermal sites have been identified [*German et al.*, 1996; *German and Parson*, 1998; *Charlou et al.*, 2000; *Dias and Barriga*, 2006]. The influence of the Azores hot spot on axial morphology and crustal thickness, however, appears to be confined to the ridge between 40° and 38°N [*Detrick et al.*, 1995]. South of ~38°N, the axis consists of deep valleys with little indication of recent volcanic activity [*German et al.*, 1996], quite unlike any of the other five hot spot–affected ridge sections considered here. All known hydrothermal activity occurs south of 37°50′N in highly tectonized areas with no neovolcanic features, frequently in the offsets between ridge segments. These settings are quite distinct from the dominantly volcanic environment of other hot spot–affected ridge sections. *German et al.* [1996] concluded that the incidence of venting south of ~38°N is controlled not by the Azores hot spot but by crustal fissuring that allows seawater access to deep heat sources. While it would be instructive to consider hydrothermal gradients along the entire 40° to 36°N section, plume data are insufficient to reliably calculate a p_h value [*Baker and German*, 2004], making quantitative comparisons to other ridge sections unworkable. No hydrothermal surveys between 40° and 38°N have been published, and surveys farther south have been conducted only by widely spaced vertical casts [e.g., *Chin et al.*, 1998] or by deep tows with a single optical sensor [e.g., *German et al.*, 1996].

[25] The Iceland hot spot is the most prominent example of an on-ridge hot spot [*Courtillot et al.*, 2003], having an along-axis bathymetric anomaly extending >2500 km [*Ito and Lin*, 1995]. The axial high topography and abundant axial volcanic ridges of the Reykjanes Ridge are unique for a slow-spreading ridge [*Searle et al.*, 1998]. Crustal thickness increases from ~9 km at 58°N [*Sinha et al.*, 1998] to ~12 km at 62°N [*Smallwood et al.*, 1995]. *German et al.* [1994] occupied 175 vertical profiles along 750 km of ridge from 57°45′ to 63°09′N, collecting optical and chemical data at each. Evidence of only a single vent site was found (at 63°06′N), yielding a p_h = 0.012. Surprisingly, no hydrothermal plume evidence was found near 57°45′N [*German and Parson*, 1998], where an AMC only 2–3 km below the seafloor was later imaged [*Sinha et al.*, 1998].

[26] The St. Paul-Amsterdam hot spot is located some 100 km west of the SEIR and has constructed a 150 km by 200 km volcanic massif astride the ridge, increasing the local crustal thickness to 10–12 km [*Scheirer et al.*, 2000]. No AMC surveys have been conducted here. While no continuous survey of plumes exists, *Scheirer et al.* [1998] collected 58 vertical ΔNTU profiles along 445 km of ridge within the hot spot massif. A minimum of two and a maximum of four profiles detected plumes, for a p_h = 0.034 to 0.069, substantially lower than expected for a spreading rate of 66 mm/a [*Baker and German*, 2004]. Six of 35 profiles taken on SEIR sections off the massif detected plumes, for a p_h = 0.171.

[27] The designation of Ascension as a true hot spot has been long debated. The MAR between the Ascension (7°30′S) and Bode Verde (11°30′S) fracture zones shows a ~1 km depth anomaly [*Minshull et al.*, 2003] and geochemical anomalies in basalt layer 2A [*Schilling et al.*, 1985] suggestive of a hot spot influence. Crustal thickness increases to ~11 km between 9° and 10°S [*Bruguier et al.*, 2003], where the axial valley transitions to a rifted axial high. This transition is similar to that seen between 95° and 91°W on the GSC. *Bruguier et al.* [2003] argue that the geophysical and geochemical anomalies simply result from the melting of small (<200 km) mantle heterogeneities; no elevated mantle temperature is needed. Hydrothermal plumes were first mapped in 2003 by a combined deep-tow/MAPR array similar to that used along the GSC, except that the deep-tow vehicle was towed higher so the bottommost MAPR was often >100 m above bottom. The 2003 MAPR tows detected plumes at three locations along 450 km of ridge [*Devey et al.*, 2005], yielding a p_h = 0.044. Subsequent cruises using a remotely operated vehicle confirmed a vent site near 8°S first indicated by the MAPR tows [*Koschinsky et al.*, 2006] and discovered a series of low-temperature vent sites on the bathymetric minimum near 9°30′S [*Haase and Scientific Party*, 2005; *Koschinsky et*

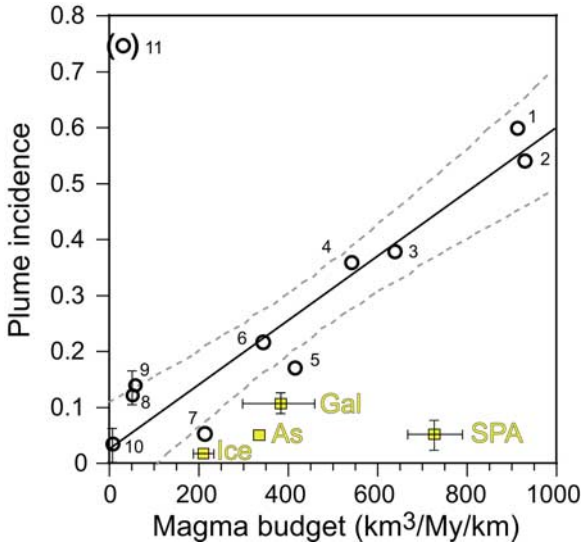

Figure 8. Scatterplot of p_h versus magma budget, V_m (spreading rate × crustal thickness), for "normal" ridge sections (black circles) and hot spot–affected ridge sections (yellow squares). Hot spot sections include "Ice," Reykjanes Ridge (58°–63°N); "As," MAR 7°–11°S; "Gal," GSC (this study); and "SPA," SEIR (37°–39.5°S). Normal ridge sections include 1, EPR 13°–18°S; 2, EPR 27°–32°S; 3, EPR 9°–13°N; 4, EPR 15°–18°N; 5, SEIR, 77°–88°E; 6, JdFR; 7, MAR 2–7°S [*German et al.*, 2005]; 8, western SWIR (58°–66°E); 9 and 10, oblique (10°–16°E) and orthogonal (16°–23°E) supersegments, respectively, of eastern SWIR; and 11, Gakkel Ridge. References for these sections are provided by *Baker et al.* [2004], except for 7. Solid line is least squares regression for normal ridges, $p_h = 0.04 + 0.00055V_m$; dotted lines are the 95% confidence bands for the slope. The Gakkel Ridge value ($p_h = 0.75$) is not used because it is inflated by unique hydrographic and bathymetric characteristics [*Baker et al.*, 2004].

al., 2006]. Since these low-temperature vents were not found by the MAPR tows (presumably because of the relatively high tow altitude), the p_h of 0.044 is likely a slight underestimate of the true plume extent.

6. Discussion

[28] The principal objective of this study was to test the hypothesis that the spatial density of hydrothermal plumes is reduced over ridge sections with thickened and warmer crust. The GSC provides a natural laboratory for this objective, since our study area ranged from crust of normal thickness and temperature to a thicker crust underlain by a warmer mantle. Results from the GSC are consistent with earlier work along the Reykjanes Ridge (Iceland hot spot), the SEIR (St. Paul-Amsterdam hot spot), and the MAR (Ascension hot spot): these ridge sections have a consistently lower incidence of detectable hydrothermal plumes compared to other ridge sections with similar magma budgets (Figure 8). A primary issue is whether these hydrothermal anomalies have a uniform explanation, or are merely coincidental in some way. In the following sections we consider the merits of three possible explanations for this observation: (1) convective cooling and consequent hydrothermal discharge is substantially reduced along ridge sections with thickened crust, (2) convective cooling is normal but expressed as widespread low-temperature discharge that is undetectable by large-scale water column surveys, and (3) the delivery of hot spot–derived magma to the crust is episodic.

6.1. Reduced Convective Cooling

[29] *Chen* [2003] first advanced the possibility of reduced convective cooling as an explanation for the remarkable absence of detected vent emissions along 750 km of the Reykjanes Ridge [*German et al.*, 1994]. He quantified this suggestion by expressing hydrothermal cooling as a decrease in the ratio of convective to conductive cooling, or Nusselt number, Nu. At the Reykjanes Ridge, for a $\Delta T = 40°C$, a decrease in Nu from 8 (typical for "normal" ridges) to 2 permits the permanent maintenance of a shallow AMC at the 2.5 km depth imaged by *Sinha et al.* [1998]. *Chen* [2003] suggested that hydrothermal circulation and convective cooling might be reduced along the Reykjanes Ridge because increased mantle temperatures produce a hotter, more ductile crust, reducing fracturing and thus permeability. The thermal model of *Chen* [2003] predicts that reducing Nu increases crustal temperatures above the AMC by about threefold because of increased latent heat in the AMC.

[30] The GSC tests the predictions of the crustal thermal model on a larger spatial scale. *Chen and Lin* [2004] used the model to reproduce the observed changes in AMC depth between 92° and 94°W. The conditions at 92°W, assumed to be a ΔT of 30°C and normal (Nu = 8) cooling, produce a steady state AMC at ~2 km depth. For a ΔT of 20°C [*Cushman et al.*, 2004], however, slightly reduced cooling (Nu = 6) might be needed to achieve the observed AMC depth. At 94°W, a ΔT of 0° and Nu = 8 produce an AMC at ~3.4 km,

close to the observed depth. At neither location is substantially reduced hydrothermal cooling (lower Nu) needed to generate a model AMC that matches the observations.

[31] *Chen and Lin* [2004] emphasized that the simple nature of their model cannot explain either a large fluctuation in AMC depth over a short distance (such as at 91°35′ and 94°W, though these fluctuations may at least in part be related to off-axis ship wander [*Blacic et al.*, 2004]), or an abrupt change from a consistently shallow to a consistently deep AMC (such as near 92°40′W). They suggested that such variability might imply high-resolution differences in magma supply or hydrothermal cooling. Our observed distribution of p_h does not support the present level of hydrothermal cooling as a primary agent in any of these AMC fluctuations. No increase in plume occurrence accompanies the AMC deepening at 91°35′W, no unusual absence of plumes accompanies the AMC shallowing at 94°W, and no significant difference exists in p_h east and west of the depth change at 94°40′W. For the model to apply, these AMC changes must reflect small changes in the magma supply, which in the model is governed by ΔT (for a given spreading rate).

[32] Thus at the Reykjanes Ridge site, the plume observations support the reduced cooling required for a shallow AMC. Along the multisegment GSC, however, the reduction in hydrothermal cooling implied by the observed plume scarcity is not consistent with the pattern of AMC depth variations.

6.2. Low-Temperature Cooling

[33] An alternative explanation is that cooling is not reduced along hot spot–affected ridge sections but instead expressed as diffuse, and difficult to detect, low-temperature fluids. *German and Parson* [1998] proposed this explanation for the near absence of venting along the Reykjanes Ridge, and offered two possible explanations for why low-temperature fluids might dominate the cooling process. First, low-temperature, metal-poor discharge might arise because of widespread low-temperature phase separation at the relatively shallow depths of the Reykjanes Ridge. This explanation suffers both from the fact that the single field found was at the shallowest end of the ridge and yet did emit a metal-rich plume, and that other, deeper, hot spot–affected ridges also have abnormally low p_h values (though not as low as the Reykjanes Ridge).

[34] *German and Parson*'s [1998] second suggestion is that excessive dilution of hydrothermal fluids by seawater in high-porosity crustal rocks might lower discharge temperatures, precipitate particle-forming metals in the crust, and produce weak, inconspicuous plumes. Evidence for high crustal porosity above the Reykjanes AMC site comes from a joint interpretation of seismic and electromagnetic data that implies a highly interconnected fluid phase is present there [*Greer et al.*, 2002]. *MacGregor et al.* [2002] used this same technique at the Valu Fa Ridge in the Lau Basin, and found porosity even higher than at the Reykjanes Ridge. At the Valu Fa, however, hydrothermal plumes are widespread [*Baker et al.*, 2006] and high-temperature vents common [*Tivey et al.*, 2005], so increased porosity alone is not likely to eliminate the development of high-temperature discharge.

[35] If diffuse, low-temperature fields do dominate convective cooling along the GSC, they must be of a scale that cannot be detected even with our unusually detailed sampling. Throughout 157 h of camera tows, virtually all diffuse discharge was associated with the black smoker fields (Haymon et al., submitted manuscript, 2008). Around the 9°50′N vent fields on the East Pacific Rise, *Ramondenc et al.* [2006] commonly observed large (~25 m^2) patches of diffuse flow, with mean exit temperatures of ~10°C. If such fields were isolated from black smoker sites (unlike on the East Pacific Rise) they would have been difficult to detect even in our detailed survey. In fact, DSL-3 was unable to detect the Calyfield vent site near 89°36′W, a 60 m × 60 m field, discovered by the submersible *Alvin*, producing only weak and low-temperature diffuse discharge [*Yoerger et al.*, 2002]. Until the true extent of diffuse discharge is quantified, its importance to axial cooling of hot spot–affected ridge sections will remain unresolved.

6.3. Episodic Melt Delivery

[36] A simple explanation for the low p_h we observed on the GSC is that the hot spot influence is not steady but episodic, with the GSC-wide (i.e., ~95°–89°E) magma supply rate fluctuating over time, or with melt delivery to the seafloor fluctuating via coeval episodes of dike intrusion along multiple segments (Haymon et al., submitted manuscript, 2008). The presence of an AMC along most of our study area suggests that it is melt delivery to the seafloor, rather than melt supply to the crust, that may be episodic. The observation

that all four hot spot ridges in Figure 8 have a reduced p_h demands that each one is presently in a period of quiescent magma delivery (or supply). This coincidence could reasonably occur only if active periods are rare and the hydrothermal activity they engender is brief. Haymon et al. (submitted manuscript, 2008) examine in detail the issue of large-scale temporal variability in the magmatic budget at hot spot–affected ridge sections.

7. Conclusions

[37] Our detailed plume survey along the portion of the GSC most affected by the Galápagos hot spot confirms that detectable (i.e., largely high temperature) hydrothermal plumes are significantly scarcer than along non–hot spot–affected ridge sections with similar magma budgets. Some low-temperature sites discharging plumes of weak buoyancy flux could have gone undetected, but there is little likelihood that there are additional high-temperature fields beyond the two confirmed and one inferred sites discovered. These results support earlier, less detailed surveys along hot spot–affected sections of the Reykjanes, South East Indian, and Mid-Atlantic Ridges where low incidences of plumes were also found.

[38] The cause, or causes, of apparently weak hydrothermal activity on these ridge sections remains uncertain. Results from the Reykjanes Ridge are consistent with a strong reduction in hydrothermal cooling, as required by a crustal thermal model [*Chen and Lin*, 2004] to maintain a shallow AMC there. But the model is not consistent with the low cooling implied by the low plume incidence observed along the GSC, where calculated changes in mantle temperature are sufficient to cause the observed changes in AMC depth.

[39] A second alternative is that hydrothermal cooling is not in fact reduced on these ridge sections, but instead occurs largely as difficult-to-detect, low-temperature diffuse flow. This alternative satisfies the crustal thermal model. However, there is no observational evidence that substantial diffuse fields, unaccompanied by nearby high-temperature discharge, commonly occur along the GSC or other ridge sections. Finally, it is conceivable that the delivery of melt by hot spots or mantle melting anomalies is episodic on long timescales. The four hot spot–affected ridge sections known to have a low spatial density of hydrothermal plumes may simply be fortuitously quiescent at present. Haymon et al. (submitted manuscript, 2008) examine the details of this argument.

[40] The scarcity of detectable hydrothermal plumes along hot spot–affected ridge sections now has a convincing observational base, but may [*Chen*, 2003] or may not [*Chen and Lin*, 2004] be compatible with explanations based on their crustal thermal model. Determining the cause of these observations awaits an expanded database of seismic and hydrothermal observations along multiple hot spot–affected ridge sections. For example, the shallow depth of the AMC at 57°45′N on the Reykjanes Ridge is consistent with reduced convective cooling, but a lengthier survey for melt along the Reykjanes Ridge is needed to fully confirm the applicability of the crustal thermal model there. The greatest need for additional hydrothermal observations on hot spot–affected ridges is conclusive evidence about the extent of low-temperature discharge. This is a daunting logistical challenge that will not be practical until efficient and affordable autonomous underwater vehicles are standard oceanographic equipment.

Acknowledgments

[41] We thank the *T.G. Thompson*, the many students and technicians who participated in the data collection efforts, and the government of Ecuador for permission to work in its national waters and EEZ. This research was jointly funded by the National Science Foundation (OCE-0324668 to R.M.H. and K.C.M.; OCE-0326148 to S.M.W.; OCE-0326272 to J.A.R.; OCE-0324232 to T. Shank) and by NOAA's Office of Ocean Exploration and VENTS Program (NOAA-OE grant NA04OAR600049). This is JISAO contribution 1311 and PMEL contribution 3189.

References

American Public Health Association (1985), *Standard Methods for the Examination of Water and Wastewater*, 16th ed., APHA, AWWA, and WPCF joint publication, 1268 pp., Washington, D. C.

Anderson, D. L., T. Tanimoto, and Y. Zhang (1992), Plate tectonics and hotspots: The third dimension, *Science*, *256*, 1645–1651, doi:10.1126/science.256.5064.1645.

Baker, E. T., and C. R. German (2004), On the global distribution of hydrothermal vent fields, in *Mid-Ocean Ridges: Hydrothermal Interactions Between the Lithosphere and Oceans*, *Geophys. Monogr. Ser.*, vol. 148, edited by C. R. German, J. Lin, and L. M. Parson, pp. 245–266, AGU, Washington, D. C.

Baker, E. T., and S. R. Hammond (1992), Hydrothermal venting and the apparent magmatic budget of the Juan de Fuca Ridge, *J. Geophys. Res.*, *97*, 3443–3456, doi:10.1029/91JB02671.

Baker, E. T., and H. B. Milburn (1997), MAPR: A new instrument for hydrothermal plume mapping, *RIDGE Events*, *8*, 23–25.

Baker, E. T., H. N. Edmonds, P. J. Michael, W. Bach, H. J. B. Dick, J. E. Snow, S. L. Walker, N. R. Banerjee, and C. H. Langmuir (2004), Hydrothermal venting in magma deserts: The ultraslow-spreading Gakkel and South West Indian Ridges, *Geochem. Geophys. Geosyst.*, *5*(8), Q08002, doi:10.1029/2004GC000712.

Baker, E. T., J. A. Resing, S. L. Walker, F. Martinez, B. Taylor, and K. Nakamura (2006), Abundant hydrothermal venting along melt-rich and melt-free ridge segments in the Lau back-arc basin, *Geophys. Res. Lett.*, *33*, L07308, doi:10.1029/2005GL025283.

Blacic, T. M., G. Ito, J. P. Canales, R. S. Detrick, and J. Sinton (2004), Constructing the crust along the Galapagos Spreading Center 91.3°–95.5°W: Correlation of seismic layer 2A with axial magma lens and topographic characteristics, *J. Geophys. Res.*, *109*, B10310, doi:10.1029/2004JB003066.

Bruguier, N. J., T. A. Minshull, and J. M. Brozena (2003), Morphology and tectonics of the Mid-Atlantic Ridge, 7°–12°S, *J. Geophys. Res.*, *108*(B2), 2093, doi:10.1029/2001JB001172.

Canales, J. P., G. Ito, R. S. Detrick, and J. Sinton (2002), Crustal thickness along the western Galápagos Spreading Center and the compensation of the Galápagos hotspot swell, *Earth Planet. Sci. Lett.*, *203*, 311–327, doi:10.1016/S0012-821X(02)00843-9.

Charlou, J. L., J. P. Donval, E. Douville, P. Jean-Baptiste, J. Radford-Knoery, Y. Fouquet, A. Dapoigny, and M. Stievenard (2000), Compared geochemical signatures and the evolution of Menez Gwen (37°50′ N) and Lucky Strike (37°17′ N) hydrothermal fluids, south of the Azores Triple Junction on the Mid-Atlantic Ridge, *Chem. Geol.*, *171*, 49–75, doi:10.1016/S0009-2541(00)00244-8.

Chen, Y. J. (1992), Oceanic crustal thickness versus spreading rate, *Geophys. Res. Lett.*, *19*, 753–756, doi:10.1029/92GL00161.

Chen, Y. J. (2003), Influence of the Iceland mantle plume on crustal accretion at the inflated Reykjanes Ridge: Magma lens and low hydrothermal activity?, *J. Geophys. Res.*, *108*(B11), 2524, doi:10.1029/2001JB000816.

Chen, Y. J., and J. Lin (2004), High sensitivity of ocean ridge thermal structure to changes in magma supply: The Galápagos Spreading Center, *Earth Planet. Sci. Lett.*, *221*, 263–273, doi:10.1016/S0012-821X(04)00099-8.

Chin, C. S., G. P. Klinkhammer, and C. Wilson (1998), Detection of hydrothermal plumes on the northern Mid-Atlantic Ridge: Results from optical measurements, *Earth Planet. Sci. Lett.*, *162*, 1–13, doi:10.1016/S0012-821X(98)00141-1.

Christie, D. M., R. Werner, F. Hauff, K. Hoernle, and B. B. Hanan (2005), Morphological and geochemical variations along the eastern Galápagos Spreading Center, *Geochem. Geophys. Geosyst.*, *6*, Q01006, doi:10.1029/2004GC000714.

Corliss, J. B., et al. (1979), Submarine thermal springs on the Galápagos Rift, *Science*, *203*, 1073–1083, doi:10.1126/science.203.4385.1073.

Courtillot, V., A. Davaille, J. Besse, and J. Stock (2003), Three distinct types of hotspots in the Earth's mantle, *Earth Planet. Sci. Lett.*, *205*, 295–308, doi:10.1016/S0012-821X(02)01048-8.

Cushman, B., J. Sinton, G. Ito, and J. Eaby Dixon (2004), Glass compositions, plume-ridge interaction, and hydrous melting along the Galápagos Spreading Center, 90.5°W to 98°W, *Geochem. Geophys. Geosyst.*, *5*, Q08E17, doi:10.1029/2004GC000709.

DeMets, C., R. G. Gordon, D. F. Argus, and S. Stein (1994), Effect of recent revisions to the geomagnetic reversal time scale on estimates of current plate motions, *Geophys. Res. Lett.*, *21*, 2191–2194, doi:10.1029/94GL02118.

Detrick, R. S., H. D. Needham, and V. Renard (1995), Gravity anomalies and crustal thickness along the Mid-Atlantic Ridge between 33°N and 40°N, *J. Geophys. Res.*, *100*, 3767–3787, doi:10.1029/94JB02649.

Detrick, R. S., J. M. Sinton, G. Ito, J. P. Canales, M. Behn, T. Blacic, B. Cushman, J. E. Dixon, D. W. Graham, and J. Mahoney (2002), Correlated geophysical, geochemical and volcanological manifestations of plume-ridge interaction along the Galápagos Spreading Center, *Geochem. Geophys. Geosyst.*, *3*(10), 8501, doi:10.1029/2002GC000350.

Devey, C. W., K. S. Lackschewitz, and E. T. Baker (2005), Hydrothermal and volcanic activity found on the southern Mid-Atlantic Ridge, *Eos Trans. AGU*, *86*(22), 209.

Dias, A. S., and F. J. A. S. Barriga (2006), Mineralogy and geochemistry of hydrothermal sediments from the serpentinite-hosted Saldanha hydrothermal field (36°34′N; 33°26′W) at MAR, *Mar. Geol.*, *225*, 157–175, doi:10.1016/j.margeo.2005.07.013.

Dyment, J., J. Lin, and E. T. Baker (2007), Ridge-hotspot interactions—What mid-ocean ridges tell us about deep Earth processes, *Oceanography*, *20*, 102–115.

German, C. R., and L. M. Parson (1998), Distributions of hydrothermal activity along the Mid-Atlantic Ridge: Interplay of magmatic and tectonic controls, *Earth Planet. Sci. Lett.*, *160*, 327–341, doi:10.1016/S0012-821X(98)00093-4.

German, C. R., et al. (1994), Hydrothermal activity on the Reykjanes Ridge: The Steinahóll Vent-field at 63°06′N, *Earth Planet. Sci. Lett.*, *121*, 647–654, doi:10.1016/0012-821X(94)90098-1.

German, C. R., L. M. Parson, and the HEAT Scientific Team (1996), Hydrothermal exploration at the Azores Triple-Junction: Tectonic control of venting at slow-spreading ridges?, *Earth Planet. Sci. Lett.*, *138*, 93–104, doi:10.1016/0012-821X(95)00224-Z.

German, C., et al. (2005), Hydrothermal activity on the southern Mid-Atlantic Ridge: Tectonically- and volcanically-hosted high temperature venting at 2–7°S, *Eos Trans. AGU*, *86*(52), Fall Meet. Suppl., Abstract OS21C-04.

Greer, A. A., M. C. Sinha, and L. M. MacGregor (2002), Joint effective medium modeling for co-incident seismic and electromagnetic data, and its application to studies of porosity structure at mid-ocean ridge crests, in *Lithos Science Report April 2002*, vol. 4, edited by S. C. Singh, P. J. Barton, and M. C. Sinha, pp. 103–120, Univ. of Cambridge, Cambridge, U. K.

Haase, K. M., and Scientific Party (2005), Hydrothermal activity and volcanism on the southern Mid-Atlantic Ridge, *Eos Trans. AGU*, *86*(52), Fall Meet. Suppl., Abstract OS21C-05.

Haymon, R., S. M. White, E. T. Baker, P. G. Anderson, K. C. Macdonald, and J. A. Resing (2008), High-resolution surveys along the hot spot–affected Galápagos Spreading Center: 3. Black smoker discoveries and the implications for geological controls on hydrothermal activity, *Geochem. Geophys. Geosyst.*, doi:10.1029/2008GC002114, in press.

Hey, R., et al. (2004), Tectonic/volcanic segmentation and controls on hydrothermal venting along Earth's fastest seafloor spreading system, EPR 27°–32°S, *Geochem. Geophys. Geosyst.*, *5*, Q12007, doi:10.1029/2004GC000764.

Hooft, E., and R. Detrick (1995), Relationship between axial morphology, crustal thickness, and mantle temperature along the Juan de Fuca and Gorda Ridges, *J. Geophys. Res.*, *100*, 22,499–22,508, doi:10.1029/95JB02502.

Ito, G., and J. Lin (1995), Oceanic spreading center-hotspot interactions: Constraints from along-isochron bathymetric and gravity anomalies, *Geology*, *23*, 657–660, doi:10.1130/0091-7613(1995)023<0657:OSCHIC>2.3.CO;2.

Ito, G., J. Lin, and D. Graham (2003), Observational and theoretical studies of the dynamics of mantle plume–mid-ocean ridge interaction, *Rev. Geophys.*, *41*(4), 1017, doi:10.1029/2002RG000117.

Koschinsky, A., C. Devey, D. Garbe-Schönberg, C. German, D. Yoerger, T. Shank, and RV Meteor M68/1 Science Party (2006), Hydrothermal exploration of the Mid-Atlantic Ridge, 5–10°S, using the AUV ABE and the ROV Quest—A brief overview of RV Meteor cruise M68/1, *Eos Trans. AGU*, *87*(52), Fall Meet. Suppl., Abstract OS34A-05.

MacGregor, L. M., A. A. Greer, M. C. Sinha, and C. Peirce (2002), Properties of crustal fluids at the Valu Fa Ridge, Lau Basin, and their relationship to active hydrothermal circulation, from joint analysis of electromagnetic and seismic data, in *Lithos Science Report April 2002*, vol. 4, edited by S. C. Singh, P. J. Barton, and M. C. Sinha, pp. 121–130, Univ. of Cambridge, Cambridge, U. K.

Massoth, G. J., E. T. Baker, R. A. Feely, J. E. Lupton, R. W. Collier, J. F. Gendron, K. K. Roe, S. M. Maenner, and J. A. Resing (1998), Manganese and iron in hydrothermal plumes resulting from the 1996 Gorda Ridge event, *Deep Sea Res., Part II*, *45*, 2683–2712, doi:10.1016/S0967-0645(98)00089-7.

Minshull, T. A., N. J. Bruguier, and J. M. Brozena (2003), Seismic structure of the Mid-Atlantic Ridge, 8–9°S, *J. Geophys. Res.*, *108*(B11), 2513, doi:10.1029/2002JB002360.

Morgan, W. J. (1971), Convection plumes in the lower mantle, *Nature*, *230*, 42–43, doi:10.1038/230042a0.

Perfit, M. R., and W. W. Chadwick (1998), Magmatism at mid-ocean ridges: Constraints from volcanological and geochemical investigations, in *Faulting and Magmatism at Mid-Ocean Ridges*, *Geophys. Monogr. Ser.*, vol. 106, edited by W. R. Buck et al., pp. 59–116, AGU, Washington, D. C.

Ramondenc, P., L. N. Germanovich, K. L. Von Damm, and R. P. Lowell (2006), The first measurements of hydrothermal heat output at 9°50′N, East Pacific Rise, *Earth Planet. Sci. Lett.*, *245*, 487–497, doi:10.1016/j.epsl.2006.03.023.

Resing, J., E. Baker, G. Lebon, S. Walker, R. Haymon, K. Nakamura, and J. Lupton (2006), The chemistry of hydrothermal plumes along the Galápagos Spreading Center, *Eos Trans. AGU*, *87*(52), Fall Meet. Suppl., Abstract V14A-08.

Scheirer, D. S., E. T. Baker, and K. T. M. Johnson (1998), Detection of hydrothermal plumes along the Southeast Indian Ridge near the Amsterdam-St. Paul hotspot, *Geophys. Res. Lett.*, *25*, 97–100, doi:10.1029/97GL03443.

Scheirer, D. S., D. W. Forsyth, J. A. Conder, M. A. Eberle, S.-H. Hung, K. T. M. Johnson, and D. W. Graham (2000), Anomalous seafloor spreading of the Southeast Indian Ridge near the Amsterdam-St. Paul Plateau, *J. Geophys. Res.*, *105*, 8243–8262, doi:10.1029/1999JB900407.

Schilling, J.-G. (1975), Azores mantle blob: Rare-earth evidence, *Earth Planet. Sci. Lett.*, *25*, 103–115, doi:10.1016/0012-821X(75)90186-7.

Schilling, J.-G., M. B. Bergeron, and R. Evans (1980), Halogens in the mantle beneath the north Atlantic, *Philos. Trans. R. Soc. London, Ser. A*, *297*, 147–178, doi:10.1098/rsta.1980.0208.

Schilling, J. G., G. Thompson, R. Kingsley, and S. Humphris (1985), Hotspot-migrating ridge interaction in the South Atlantic, *Nature*, *313*, 187–191, doi:10.1038/313187a0.

Searle, R. C., J. A. Keeton, R. B. Owens, R. S. White, R. Mecklenburgh, B. Parsons, and S. M. Lee (1998), The Reykjanes Ridge: Structure and tectonics of a hot-spot-influenced, slow-spreading ridge, from multibeam bathymetry, gravity, and magnetic investigations, *Earth Planet. Sci. Lett.*, *160*, 463–478, doi:10.1016/S0012-821X(98)00104-6.

Sinha, M. C., S. C. Constable, C. Peirce, A. White, G. Heinson, L. M. MacGregor, and D. A. Navin (1998), Magmatic processes at slow spreading ridges: Implications of the RAMESSES experiment at 57°45′N on the Mid-Atlantic Ridge, *Geophys. J. Int.*, *135*, 731–745, doi:10.1046/j.1365-246X.1998.00704.x.

Sinton, J., R. Detrick, J. P. Canales, G. Ito, and M. Behn (2003), Morphology and segmentation of the western Galápagos Spreading Center, 90.5°–98°W: Plume-ridge interaction at an intermediate spreading ridge, *Geochem. Geophys. Geosyst.*, *4*(12), 8515, doi:10.1029/2003GC000609.

Smallwood, J. R., R. S. White, and T. A. Minshull (1995), Seafloor spreading in the presence of the Iceland plume: The structure of the Reykjanes Ridge at 61°40′N, *J. Geol. Soc.*, *152*, 1023–1029.

Tivey, M. K., P. Craddock, J. Seewald, V. Ferrini, S. Kim, M. Mottl, N. A. Sterling, A. Reysenbach, and C. G. Wheat (2005), Characterization of six vent fields within the Lau Basin, *Eos Trans. AGU*, *86*(52), Fall Meet. Suppl., Abstract T31A-0477.

Walker, S. L., E. T. Baker, J. A. Resing, K. Nakamura, and P. D. McLain (2007), A new tool for detecting hydrothermal plumes: An ORP sensor for the PMEL MAPR, *Eos Trans. AGU*, *88*(52), Fall Meet. Suppl., Abstract V21D-0753.

West, M., W. Menke, M. Tolstoy, S. Webb, and R. Sohn (2001), Magma storage beneath Axial volcano on the Juan de Fuca mid-ocean ridge, *Nature*, *413*, 833–836, doi:10.1038/35101581.

West, M., W. Menke, and M. Tolstoy (2003), Focused magma supply at the intersection of the Cobb hotspot and the Juan de Fuca ridge, *Geophys. Res. Lett.*, *30*(14), 1724, doi:10.1029/2003GL017104.

White, R. S., D. McKenzie, and R. K. O'Nions (1992), Oceanic crustal thickness from seismic measurements and rare earth element inversions, *J. Geophys. Res.*, *97*, 19,683–19,715, doi:10.1029/92JB01749.

White, S. M., J. D. Meyer, R. M. Haymon, K. C. Macdonald, and J. A. Resing (2008), High-resolution surveys along the hot spot–affected Galápagos Spreading Center: 2. Influence of magma supply on volcanic morphology, *Geochem. Geophys. Geosyst.*, doi:10.1029/2008GC002036, in press.

Wilson, J. T. (1963), A possible origin for the Hawaiian Islands, *Can. J. Phys.*, *41*, 863–870.

Yoerger, D. R., R. Collier, and A. M. Bradley (2002), Hydrothermal vent plume discovery and survey with an autonomous underwater vehicle, *Eos Trans. AGU*, *83*(47), Fall Meet. Suppl., Abstract T11C-1261.